Lorandite from Allchar as geochemical detector for pp-solar neutrinos

Miodrag K. Pavićević [a], Georg Amthauer [a], Vladica Cvetković [b], Blazo Boev [c], Vladan Pejović [d], Walter F. Henning [e], Fritz Bosch [f,1], Yuri A. Litvinov [f,*], Reinhard Wagner [a]

[a] *University of Salzburg, Department of Chemistry and Physics of Materials, Jakob-Haringer-Str. 2a, 5020 Salzburg, Austria*
[b] *University of Belgrade, Faculty of Mining and Geology, Studentski Trg 16/III, 11000 Belgrade, Serbia*
[c] *University of Štip, Faculty of Mining and Geology, Goce Delčev 89, 92000 Štip, Former Yugoslav Republic of Macedonia, The*
[d] *Institute of Physics, Zemun, Pregrevica 118, 11000 Belgrade, Serbia*
[e] *Argonne National Laboratory, Physics Division, Argonne, IL, USA*
[f] *GSI Helmholtzzentrum für Schwerionenforschung, Planckstr. 1, 64291 Darmstadt, Germany*

A B S T R A C T

Keywords:
Lorandite
Geochemical neutrino detector
Allchar ore deposit
pp-solar neutrinos

LOREX (LORandite EXperiment) is a geochemical project addressing the solar proton–proton neutrino flux for the period of 4.31(2) Ma from the reaction $^{205}Tl + \nu_e \rightarrow {}^{205}Pb + e^-$ with a very low threshold (52 keV) for solar pp-neutrino capture. A decisive step for this purpose is to obtain the precise, background-corrected ratio of $^{205}Pb/^{205}Tl$ in the mineral lorandite ($TlAsS_2$) as geochemical detector occurring in the ore deposit of Allchar in Macedonia. This study presents a report on the excavation of lorandite bearing ore from adit P-21 of the ore body Crven Dol as well as on the separation of pure lorandite from the raw ore. A detailed mineralogical and chemical investigation of the separated lorandite is performed with special regard to the question of its use as detector for solar pp-neutrinos.

1. Introduction

### 1.1. The lorandite experiment (LOREX), short history and neutrino detection

In 1894, Krenner discovered a new mineral from the Allchar ore deposit with the chemical formula $TlAsS_2$ and named it lorandite in honor of the Hungarian physicist Eötvös Lorand [1]. Crystal data, physical and optical properties, cell data, occurrences, and other characteristics of lorandite can be found in [2]. Some lorandite crystals from adit P-21 of the mine of Crven Dol in the Allchar ore deposit are shown in Fig. 1.

In the seventies, [3] proposed to use lorandite from the Allchar ore deposit as a new test for solar neutrinos based on the neutrino (ν_e) capture by the ^{205}Tl isotope and its transformation to the radionuclide ^{205}Pb, which also includes the emission of an electron (see below). H. Morinaga, E. Nolte (both TU Munich) and M.K. Pavićević (University of Belgrade) proposed the project "Application of Thallium Minerals as Solar Neutrino Detectors".

Between 1985 and 1990 three international conferences were organized and realized: (i) Workshop on "the Feasibility of the Solar Neutrino Detection with ^{205}Tl" from 23th till 24th September 1985 in Munich, (ii) International Conference on "Solar Neutrino Detection with

^{205}Tl and Related Topics" from 29th September till 3rd October 1986 in Dubrovnik and (iii) "Thallium Neutrino Detection 1990 International Symposium on Solar Neutrino Detection with ^{205}Tl" from 9th till 12th October 1990 in Dubrovnik. During the International Conference 1986, M. K. Pavićević suggested LOREX as acronym for LORandit EXperiment instead of Solar Neutrino Experiment with ^{205}Tl [4]. All the results were compiled and reviewed in the paper "The "LOREX"-Project, solar neutrino detection with the mineral lorandite (Progress Report)" by [5]. Due to the civil war and the decay of former Yugoslavia, the fruitful research and the cooperation between the partners of the LOREX project were extremely hindered and almost broke down.

The physical principles of LOREX are described in detail by [4–6]. The detection principle is based on the neutrino (ν_e) capture by the ^{205}Tl isotope and the transformation to the radionuclide ^{205}Pb (half-life $T_{1/2} = 17.3(7)$ Ma [7]), which also includes the emission of an electron according to the reaction originally proposed by [3]:

$$^{205}Tl + \nu_e(\geq 52 \text{ keV}) \rightarrow {}^{205}Pb * + e^- \qquad (1)$$
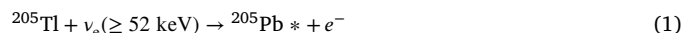
The average neutrino flux Φ_ν over the exposure time T (age of lorandite since its mineralization) follows from the common activation

---

Fig. 1. Lorandite crystals from adit P-21 Crven Dol, Allchar, Macedonia.

equation [5]:

$$\Phi_\nu \sigma_\nu = C \frac{(N^{205}Pb)_{exp} - (N^{205}Pb)_B}{m(1 - e^{\lambda T})} \tag{2}$$

where C is a constant ($C = 3.79 \times 10^{-19}$ mol a^{-1}), σ_ν is the cross section for the capture of solar pp-neutrinos by ^{205}Tl, $(N^{205}Pb)_{exp}$ is the experimentally determined number of ^{205}Pb atoms in lorandite of mass m, $(N^{205}Pb)_B$ is the number of ^{205}Pb atoms in lorandite resulting from background reactions, λ is the decay constant of ^{205}Pb ($\lambda = 4.01(16) \times 10^{-8}$ y^{-1} [7]), and $T = 4.31(2)$ Ma is the age of the thallium mineralization in the Allchar ore deposit [8]. This renders finally the mean solar pp-neutrino flux, i.e. the mean luminosity of the sun during the last 4.31(2) million years, and the geological age T of lorandite [5,9].

However, in order to obtain the real mean solar pp-neutrino flux, the solar pp-neutrino capture cross-section transmuting ^{205}Tl into ^{205}Pb has to be determined, because the ratio ^{205}Pb/^{205}Tl provides only the product of solar neutrino flux and neutrino capture probability into the different nuclear states of ^{205}Pb. The capture of neutrinos should populate predominantly the first excited state at $E^* = 2.3$ keV [10]. Its probability can be determined from the bound-state beta decay probability (β_b) according to ^{205}Tl$^{81+} \rightarrow \,^{205}$Pb $^{*81+}$ ($E^* = 2.3$ keV) + e$^-$ + $\bar{\nu}_e$, since this decay shares the same nuclear transition matrix element with the neutrino capture.

In the bound-state beta decay, the emitted electron is not emitted to continuum but is captured on one of the bound orbitals. It is therefore clear that in order to enable this decay mode, fully-ionized ^{205}Tl has to be produced and stored for extended period of time. It is proposed to employ the radioactive ion beam complex at GSI in Darmstadt. The combination of the heavy-ion synchrotron SIS, the fragment separator FRS and the experimental storage ring ESR turns out to be presently the only facility worldwide where the bound state beta decay of ^{205}Tl can be measured [11]. The feasibility of the experiment has been intensively studied in the last years. Due to construction work for the future FAIR facility, the GSI accelerators are presently in a shutdown phase. The measurement of the bound state beta decay of ^{205}Tl is one of the objectives of the ERC Consolidator Grant "ASTRUm" at GSI and is planned after the restart of the accelerator operation in 2018.

The mineralogical and geochemical study of this paper reports the results of the activities that had the following goals: (i) to reopen adit P-21 of the ore body Crven Dol in the Allchar ore deposit, (ii) to excavate lorandite bearing ore from the ore body Crven Dol, (iii) to separate lorandite as pure as possible from the raw ore, and iv) to examine if the so far extracted "pure lorandite" is really pure, with special emphasis on the contents of trace elements significant for background reactions that originate from natural radioactivity (i.e. Bi, Pb, U, and Th).

1.2. The Allchar ore deposit

The Allchar Sb–As–Tl–Au hydrothermal deposit is due to volcanic activity that mostly occurred in the Pliocene, i.e. 6.5–1.7 Ma ago [12–15]. This volcanism, which represents the youngest phase of volcanic processes that had started earlier in Mid-Miocene, produced mainly subvolcanic latite and andesite rocks. Geotectonically, the Allchar Pliocene shallow intrusive complex is situated within a NNW–SSE (North North West–South South East) stretching boundary zone between the Pelagonian geotectonic unit and the Vardar oceanic suture [16]. The basement predominantly consists of Mesozoic rocks, such as Triassic dolomite and dolomitic marble, clayey schist and limestone as well as of Jurassic serpentinized peridotite and diabase. The volcanic complex is partially covered by glacial rocks and by Pliocene to Quaternary volcano-sedimentary and alluvium deposits.

As it can be depicted from the geological map in Fig. 2, the Sb–As–Tl–Au mineralization of the Allchar deposit occurs as two ore bodies: Crven Dol and Centralni deo, which are situated within a 3 km long and 200–300 m wide zone, composed of various volcanic and sedimentary rocks. It comprises the following morphostructural types of mineralization: (i) mineralized brecciated zones which developed along the contact between the subvolcanic intrusions and adjacent rocks or along shear zones within carbonate rocks and/or silicified tuffs, (ii) massive lenses of realgar ore, which occur in carbonate rocks and grade into stockwork-type mineralization, (iii) systems of veinlets and fractures that occur in dolomite, (iv) disseminated mineralization, consisting mostly of stibnite, pyrite/marcasite and native gold, which itself shows several morphogenetic subtypes, and (v) a system of thin, up to 10 cm wide, subparallel veins of orpiment, which are identified in the Crven Dol ore body at 800 m level.

The most important elements of the deposit are Sb, As, Tl, Fe, S and Au, which are accompanied by minor contents of Hg and Ba as well as by traces of Pb, Zn, Cu, U and Th. The enrichments in gold correlate positively with enrichments in silica, while the enrichment in Tl is related to increased concentrations of As, Sb, Hg and S. The distribution of ore metals and their grades display a lateral zoning (Fig. 2): Zone I that is situated in the southern part of the deposit and is characterized by Au mineralization accompanied by variable amounts of Sb and As, Zone II in the central part, which, along with predominant Sb and Au contains significant amount of As, Tl, minor Ba, Hg, and traces of Pb; this zone is characterized by 2–3% Sb, 2% As, up to 0.4% Tl, up to 3.5 ppm Au and 435 ppm Ba, and Zone III in the northern part of the deposit, including the Crven Dol ore body; in this zone As and Tl prevail and are accompanied by minor amounts of Sb and traces of Hg and Au. The average grade in the Crven Dol ore body is 6% As, 0.3% Tl, 0.08% Sb and 0.2 ppm Au [14]. It is estimated that there are around 20 tons of thallium at the ore body Crven Dol only [17]. LOREX is now highly focused on the lorandite bearing ore body of Crven Dol in the Allchar ore deposit, because it is the most promising place from which sufficient quantities of lorandite can be provided.

1.3. New paleo-depth estimates of the Crven Dol ore body and signal to background ratio of the detector

One of the principle factors for the success of the LOREX project was to know the erosion rate as well as the paleo-depth in the Allchar area since its formation. Before we discuss the importance of the paleo-depth it is necessary to explain why we use two geological ages of the Tl-mineralization, i.e. 4.22(7) Ma [18] and 4.31(2) Ma [8]. Troesh and Frantz in [18] determined an age of 4.22(7) Ma by applying the Ar/Ar method on sanidine of the volcanic rocks close to the ore body Crven Dol in the adit P-21, which had been altered by hydrothermal activities. Therefore, the age of the Tl-mineralization in Crven Dol most probably is 4.22(7) Ma. To check this age, sericite minerals from the Rudina location close to the ore body Centralni Deo (cf. Fig. 2) have been studied by [8] applying the same method and received an age of
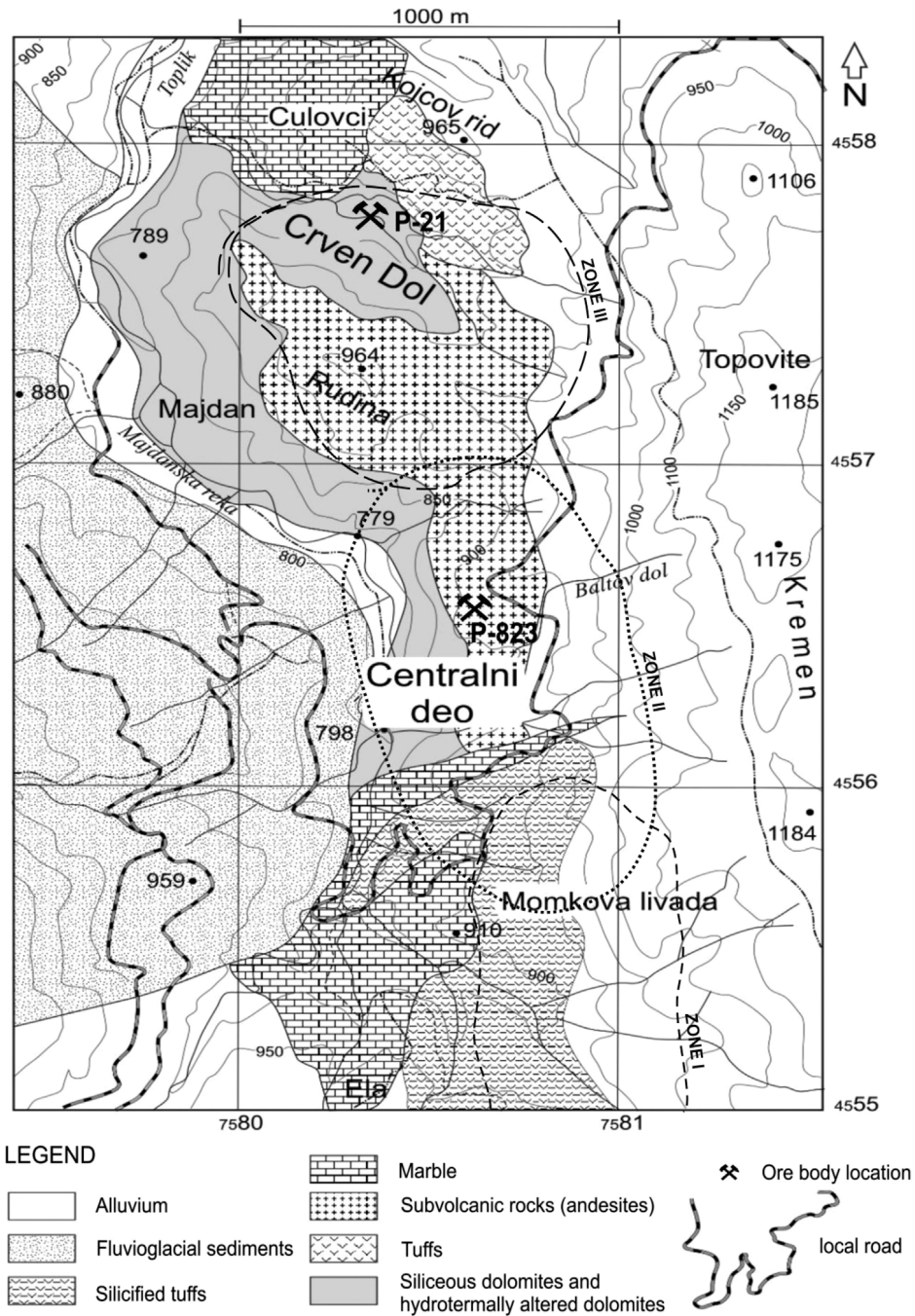
Fig. 2. Geological map of the Allchar ore deposit.

4.31(2) Ma. Because sericite also forms by hydrothermal alteration we assume that the hydrothermal ore formation in Allchar occurred at the same time. Therefore, we use the age of 4.22(7) Ma for the formation of the Crven Dol ore body and the age of 4.31(2) Ma for the whole Allchar area. However, in principle this difference between the two ages can be neglected.

Why is the knowledge of the erosion rate and the paleo-depth so important? For instance, very low erosion rates would produce a low ratio between the concentration of ^{205}Pb that is formed by pp-neutrino capture by ^{205}Tl in lorandite, which is depth-independent and the concentration of ^{205}Pb produced by so called background reactions, *i.e.* cosmic rays and natural radioactivity. Due to its short half-live as compared to the age of the Solar system, the amount of ^{205}Pb created in the s-process nucleosynthesis can safely be neglected. The ratio $[(N\ ^{205}Pb)_{exp}-(N^{205}Pb)_B]/(N\ ^{205}Pb)_B$ in lorandite is predominantly depth-dependent, which means that it depends on the average depth of the lorandite from the time when the mineralization formed to the present day, *i.e.* on paleo-depth (d_p):

$$d_p = d_{today} + 1/2\ \varepsilon \cdot T \qquad (3)$$

where d_{today} is the present day depth of the lorandite ore and ε is the average erosion rate since the time of the formation of the deposit [9].

Assuming the value of 146 SNU (Solar Neutrino Unit) for the capture rate [9], the geological age of $T = 4.31(2)$ Ma, the electron capture probability λ of ^{205}Pb back to ^{205}Tl as $\lambda = 4.01(16) \times 10^{-8}$ y^{-1} and a molar mass M of lorandite of $M = 343$ g/mol, [9] obtained the expected time-integrated number of solar electron–neutrino induced ^{205}Pb atoms,

i.e.

$$22(7) \text{ atoms of } {}^{205}\text{Pb/g lorandite}. \tag{4}$$

The newest erosion rate study in the area of the Crven Dol ore body [19] indicates higher erosion rates and higher paleo-depth values of 860 m and 2330 m, respectively, which is considerably higher than previous estimates reported by [20]. The higher erosion rate and paleo-depth values suggest a more favorable ratio between the number of atoms $(N^{205}Pb)_\nu$ originated by pp-neutrino capture and the number of atoms $(N^{205}Pb)_{fm}$ originating from the reactions induced by fast muons from cosmic rays. According to previous calculations [20], 116 atoms of ^{205}Pb in one gram of lorandite should be expected, from which 22 atoms of ^{205}Pb represent contribution of pp-neutrino capture by ^{205}Tl (Eq. (4)), and 94 atoms of ^{205}Pb represent contribution from fast muon induced reactions. Assuming the higher paleo-depth of 860 m reported by [19], about 40(9) atoms of ^{205}Pb in one gram of lorandite should be expected. From that number, 22 atoms of ^{205}Pb again represent the depth-independent contribution of pp-neutrino capture by ^{205}Tl, and 18(6) atoms of ^{205}Pb represent contribution from fast muons. Assuming that the separation efficiency of ^{205}Pb from lorandite is around 10^{-5} and that the AMS absolute detection limit δ_a of ^{205}Pb from lead is around $\leq 1 \times 10^{-3}$ [9] the minimal amount of "pure lorandite" should be about 1000 g in order to enable a successful determination of ^{205}Pb concentration.

2. Experimental

2.1. Separation of lorandite from the Crven Dol ore body

One of the major activities of LOREX was to produce sufficient quantities of pure lorandite for further experiments. In this phase, the focus was on adit P-21 of the Crven Dol ore body. According to chapter 1.3, the minimal amount of lorandite needed for further investigations is 1000 g. This is due to the absolute detection limit δ_a of the method for the detection of ^{205}Pb, which must be better than 10^{-3}, *i.e.* $\delta_a < 1 \times 10^{-3}$ [9]. The separation of lorandite from the ore body Crven Dol depends on the whole amount of lorandite within the ore body, the size of lorandite crystals and the intergrowth with other minerals, such as orpiment, realgar, gypsum, pyrite, and others. According to our estimation, the efficiency of lorandite separation is about 6.6×10^{-5}, *i.e.* in order to obtain 1 g pure lorandite, one needs to process 20 kg of lorandite bearing ore with macroscopically visible lorandite crystals.

In the following we report on

(i) the excavation of lorandite bearing ore from the ore body Crven Dol adit P-21, and on
(ii) the separation of pure lorandite from the raw ore.

2.1.1. The excavation of lorandite bearing ore from adit P-21 (Crven Dol)

According to all geological studies made until now, the ore body of Crven Dol contains the largest amount of thallium compared to all other ore bodies of the Allchar ore deposit, *i.e.* 200 tons with 0.1–0.5% Tl [14]. Unfortunately, the entrance of adit P-21 of the Crven Dol ore body is located in a completely abandoned area without road access and electrical power. The distance between the entrance of adit P-21 and the next local road is about 1.5 km. Therefore, at the beginning of our activities in fall 2014, about 1.4 km of a new forest road between the village Majdan and the entrance of adit P-21 had to be constructed.

Afterwards, the permanization of the old adit P-21 between the entrance and the ore body was started, applying the conventional Austrian tunneling method [21], *i.e.* using a wooden timbering in order to provide access to the ore body. A team of ten miners, a mining engineer and a geological engineer conducted the opening. The removal of the material in the adit was done manually, using scoop shovels and construction trolleys thus removing 120 m^3 of material. The timbering

was done using oak timbers at a distance of 50 cm. The length of the adit opening is 90 m and ended in the massive As–Tl ore body shown in detail A in Fig. 3.

The excavation of the ore was conducted manually using pneumatic hammer. The ore was excavated in the course of January 2015, around 4.5 tons, and in the course of May 2015, around 10.5 tons. The excavation was conducted by digging into the ore lenses, with on the spot visual separation, selecting the material with presumably higher concentration of lorandite. The ore was stored in metal barrels and put in the ore store in the village of Mrežičko.

Before the excavations of large amounts of lorandite-bearing ore, ten samples from the ore body of the adit P-21 were collected (see Fig. 3) and analyzed on major and trace element contents by using Inductively Coupled Plasma Mass Spectrometer (ICP-MS) (see Section 3.2). The thallium grade in the samples varied between 1 wt% and 4 wt% of Tl, displaying two sample populations one with 1–2 wt% Tl and the other with 3–4 wt% Tl. The group of samples showing the higher thallium grade was low in Ca, Mg and Sr, which indicated the lower proportion of dolomite marble in the Tl-rich ore material. Thallium contents correlated positively with Sb abundances (15–80 ppm), which suggests that thallium minerals are most likely associated with stibnite, Sb_2S_3. The correlations between thallium concentrations and the contents of other metals are very poor. For instance, a number of samples displays a positive correlation between As and Tl contents. However, there are samples with much higher arsenic contents for the given thallium concentrations, probably reflecting high abundances of realgar (± orpiment) in the raw ore.

2.1.2. The separation of pure lorandite

At the beginning of the nineties, the authors of [22] separated lorandite from the raw ore. These experiments involved mechanical grinding and a combination of gravitational (both shaking table and heavy liquids) and magnetic separation and, finally, hand picking [22]. They produced around 250 g of lorandite concentrate. However, it is difficult to assess the efficiency of the applied method, because there is no reliable information on the amount of ore that was processed for the separated amount of lorandite, on the time that was required for the preparation of the concentrate and on the ore grade of the raw ore.

Therefore, we started the separation following the approach of [22] with two pilot experiments that were carried out at the Faculty of Mining and Geology, University of Belgrade. These experiments were mutually differing in grain size distribution of pre-concentrated material. The outcomes of the experiments led to the conclusion that the method reported by [22] was not able to pre-concentrate lorandite from the raw ore. Rather than that, the grade in the processed concentrates, irrespectively of their grain size, remained very close to the grade of the starting ore. Moreover, around 60% of the starting material with a similar thallium grade (1–3% Tl) was ultimately lost in mud fractions.

LOREX could not stand such a loss in lorandite during separation, especially because of the limited amount of the available raw ore (ca 15 tons). The main conclusion was to process the entire ore almost totally manually. The new procedure took into account the following observations: (i) the overall range size of lorandite crystals is between ≥ 1 mm and < 1 cm in diameter (length), (ii) the larger crystals mostly crystallized in open space (cf. Fig. 4) or they are in physical contacts with realgar, orpiment and gypsum (*i.e.* soft minerals), whereas (iii) the smaller ones are predominantly in contact with silicates and carbonates. It therefore appears that the range in the size of lorandite crystals correlates inversely with the general hardness of the given ore rocks. This further means that if one attempts to liberate all the lorandite grains by applying the same mechanical force on the entire material (*i.e.* using a crushing and grinding device), that has the following two consequences: (1) the largest and relatively easily extractable lorandite crystals are lost forever, and (2) the produced fine-grained concentrate is not substantially enriched in lorandite.

Taking these conclusions into account, we applied a three-stage method. The first stage was carried out in Mrežičko and involved: (i)
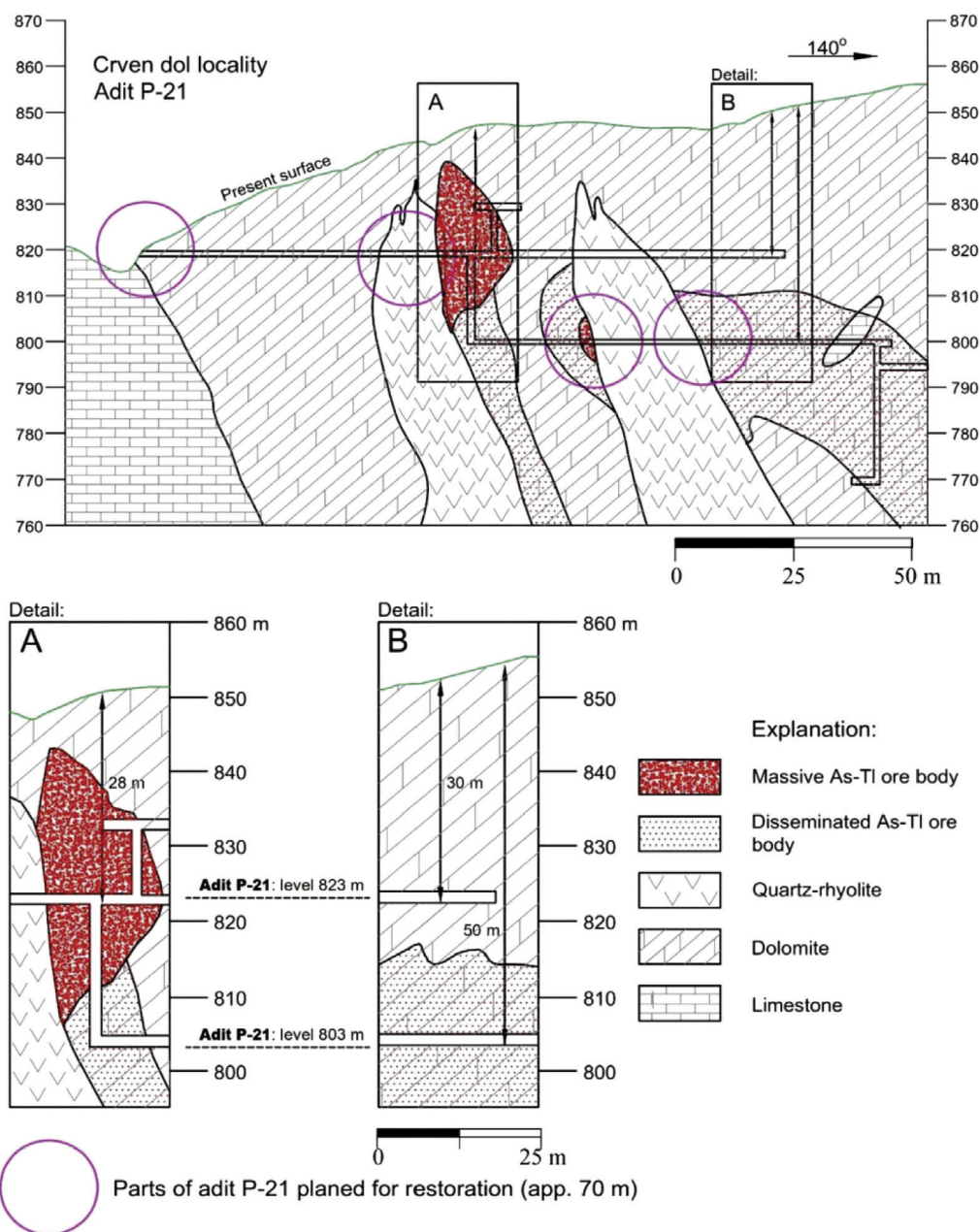
Fig. 3. Geological profile of adit P-21 Crven Dol, Allchar ore deposit.

careful examining (by naked eye and/or petrographic lens) and manual (optimized) crushing of the pristine ore, (ii) removing and disposal of the 100% barren material, (iii) thorough looking for any visible lorandite in the 'promising' ore, (iv) immediate liberation of the largest lorandite crystals (together with coatings and/or intergrowths), and (v) careful collecting (including sieving and washing) of all disintegrated material that remained after the extraction of the coarse-grained lorandite crystals. During the second stage, the previously liberated lorandite crystals were cleaned from coatings and other impurities, and simultaneously, hand picking of the most-rich fraction was carried out. The third stage focused on the finest-grained and least productive lorandite-bearing fraction, which remained from all the previous procedures. Before hand picking, this material was pre-concentrated using shaking table or magnetic separation technique. Using the approach described above, around 300 g of pure lorandite (~99%) were extracted out of ca 4.5 tons of ore. Therefore, we continued to separate lorandite from the raw ore applying the well-tried method and separated again 400 g from in total

10.5 tons of ore in approximately six to seven months of continuous work of a working team composed of eight people.

In summary, the applied method enables a continual extraction of lorandite crystals at each of separation steps and not only in the hand picking phase. In such a way, the production of the extracted lorandite is maximized whereas the loss of lorandite in the mud or dust fractions is minimized. The only disadvantage of this procedure is that the majority of large lorandite crystals must undergo careful cleaning from coatings or small inclusions and intergrowths. No matter how careful the cleaning is performed, it is virtually impossible to remove all microscopic and submicroscopic impurities by physical force and, moreover, through each step of mechanical cleaning more (purest) lorandite is lost. Even after very careful hand-picking under the binocular microscope at high magnifications, it cannot be excluded that minor amounts of extra phases occurring as inclusions or coatings are present. The amount of extra phases in the carefully prepared lorandite concentrate is estimated to be below 1.0% (see also the results of X-ray diffraction). Hence, it

Fig. 4. Lorandite crystals in the raw ore from adit P-21 Crven Dol, Allchar ore deposit.

is essential for the LOREX project to obtain information on the major impurities and how they influence the chemical composition of the lorandite concentrate. In order to address this problem, we performed a careful mineralogical and geochemical characterization of both the separated lorandite concentrates and present impurities, and the results of these investigations are reported and discussed in the following sections.

3. Results

3.1. SEM-EDS analyses

3.1.1. SEM-EDS qualitative mineralogical characterization of concentrates

Mineralogical investigations were carried out on samples of pure lorandite concentrates and on the phases that were distinguished as most frequent impurities. It was done on both unpolished grains (BSE — Backscatter Electron imaging and semi-quantitative analyses) and polished thin-sections (quantitative analyses). The investigations were performed in the Laboratory for Scanning Electron Microscopy (SEM) of the Faculty of Mining and Geology, University of Belgrade using a JEOL JSM-6610LV SEM in high vacuum conditions and with a standard tungsten filament as the source of electrons. The samples were covered by gold and/or carbon using a SCD005 sputter coating device. The chemical analyses were carried out using an Energy Dispersive System (EDS) with an X max Large Area Silicon Drift Detector (Oxford Instruments) with the application of external standards, except for thallium for which internal standards were applied. The SEM-EDS analyses of polished samples had a detection limit of 0.1 wt%.

3.1.2. SEM-EDS qualitative characterization of non-polished samples

Thirteen grains from the pure lorandite concentrate were handpicked for the SEM-EDS characterization. The selected lorandite grains had impurities that were also visible under the reflected-light binocular microscope. BSE images of two of the analyzed lorandite crystals partly coated with other phases are shown in Fig. 5. The SEM observations and EDS qualitative and semi-quantitative analyses have shown that: (i) on their clean surfaces, the lorandite grains appear homogeneous and not inter-grown with other minerals, (ii) its composition is uniform, although some semi-quantitative analyses revealed the presence of oxygen, and (iii) the phases that appear as coatings are predominantly represented by realgar, gypsum, dolomite, and mixtures of, most likely sulfates, arsenates, and other phases.

3.1.3. Quantitative analyses by EDS on polished samples

Around thirty separated grains of lorandite with or without visible extra phases were analyzed quantitatively by SEM-EDS. The results are shown in Tables 1a–1d, whereas representative BSE images for each

group of analyzed phases are shown in Fig. 5a–f. The analyses revealed the presence of pure lorandite, realgar, pyrite (marcasite), gypsum, dolomite, and a group of uncertain phases or phase mixtures.

The pure lorandite exhibits a relatively uniform chemical composition (cf. Table 1a) with an average As/Tl ratio of 0.376 ± 0.025, which is only around 2.5% higher as the lorandite stoichiometric value of As/Tl $= 0.367$ [2], i.e. within 1σ level. In agreement with the results of the semi-quantitative characterization, a majority of the quantitative SEM-EDS data show that some oxygen is present in the range of 1–2 wt%. The BSE images indicate compositional homogeneity and the absence of tiny inclusions of other phases, at least in the area of around 100×100 μm and larger (cf. Fig. 5a).

The analyzed realgar appears as tiny fresh crystals in contact with lorandite (cf. Fig. 5b). They are also compositionally homogeneous (cf. Table 1b). Except for one analysis that displays ~ 8 wt% of Tl, all other realgar grains exhibit compositions close to stoichiometry, with an average As/S ratio of 2.26 ± 0.03, only 3.5% lower of the stoichiometric As/S $= 2.34$ for realgar (within 1σ level). Gypsum occurs in aggregates of prismatic to tabular crystals (cf. Fig. 5c) that enclose tiny inclusions of, most likely, sulfides, which are also visible in translucent crystals in binocular microscope. This is maybe the reason why gypsum is compositionally more heterogeneous (cf. Table 1c) and has Ca/S ratio of 1.08 ± 0.02, around 13% lower than the stoichiometric Ca/S $= 1.25$. Moreover, most gypsum analyses contain variable contents of As, Fe, Si, Al, Mg and other elements. Two analyses in Table 1b correspond to pyrite or marcasite, whereas five analyses reported in Table 1c show the presence of dolomite some of them with almost perfect Ca/Mg ratio of around 1.66 (Fig. 5d).

The results of 17 EDS analyses in Table 1d could not be interpreted as definite mineral phases, because they did not reveal known stoichiometric compositions. They either represent so far unknown minerals or mixtures of different phases. Six analyses are compositionally similar to the "unknown" mineral reported by [23] (Fig. 5e). They suggested the following structural formula $Fe_2Tl((As_{0.85}S_{0.15})O_4)_3 \cdot 4H_2O$, which is roughly similar to the analyses reported in this study. In six other analyses O, Fe and As together make between 82 and 100 wt%. These analyses can correspond to arsenates, for instance: caribibite ($Fe_2As_4O_9$), angelilite ($Fe_4^{3+}(AsO_4)_2O_3$) or yukonite (*e.g.* $Ca_6Fe_{16}(AsO_4)_{10}(OH)_{30} \cdot 23H_2O$), although none of these minerals fits with its stoichiometric formula. The rest of the analyses most likely represent arsenates (Fig. 5f) or mixtures of various phases.

3.2. Major and trace element ICP-MS analyses

Geochemical analyses on major and trace element contents were performed using the Inductively Coupled Plasma Mass Spectrometer (ICP-MS) at the 'Goce Delčev' University of Štip.

The samples were ground by the agate mortar to obtain homogeneity of the aliquot. An amount of 0.5000 g of each sample was weighted in a glass beaker. Then, three portions of 1.5 cm^3 concentrated HNO_3 and 1.5 cm^3 H_2O_2 (both trace SELECT, Fluka) were added and the reaction mixture was heated to obtain wet salts. At the end, 2.5 cm^3 HNO_3 were added and filled up with ultrapure water in the volumetric flask of 50 cm^3.

The determination was performed by using an Agilent ICP-MS (model 7500cx). The mass used for the determination of the elements was according to the instruction by the producer of ICP-MS. The ICP-MS instrument has a system for sample introduction that consists of a dispersion chamber Quartz Scott type, a MicroMist glass concentric nebulizer and a three-channel peristaltic pump. For the efficient ionization a quartz torch was used with a diameter of injection tube of 2.5 mm. Two standard pairs of cones were inserted, the outer one made of copper and the inner one made of nickel. To obtain and support the plasma, digitally controlled 27 MHz radiofrequency generator was used. Employed was a quadrupole mass analyzer with a mass range of 2–260 AMU (atomic mass unit), a radiofrequency of 3 MHz, sensitivity to low
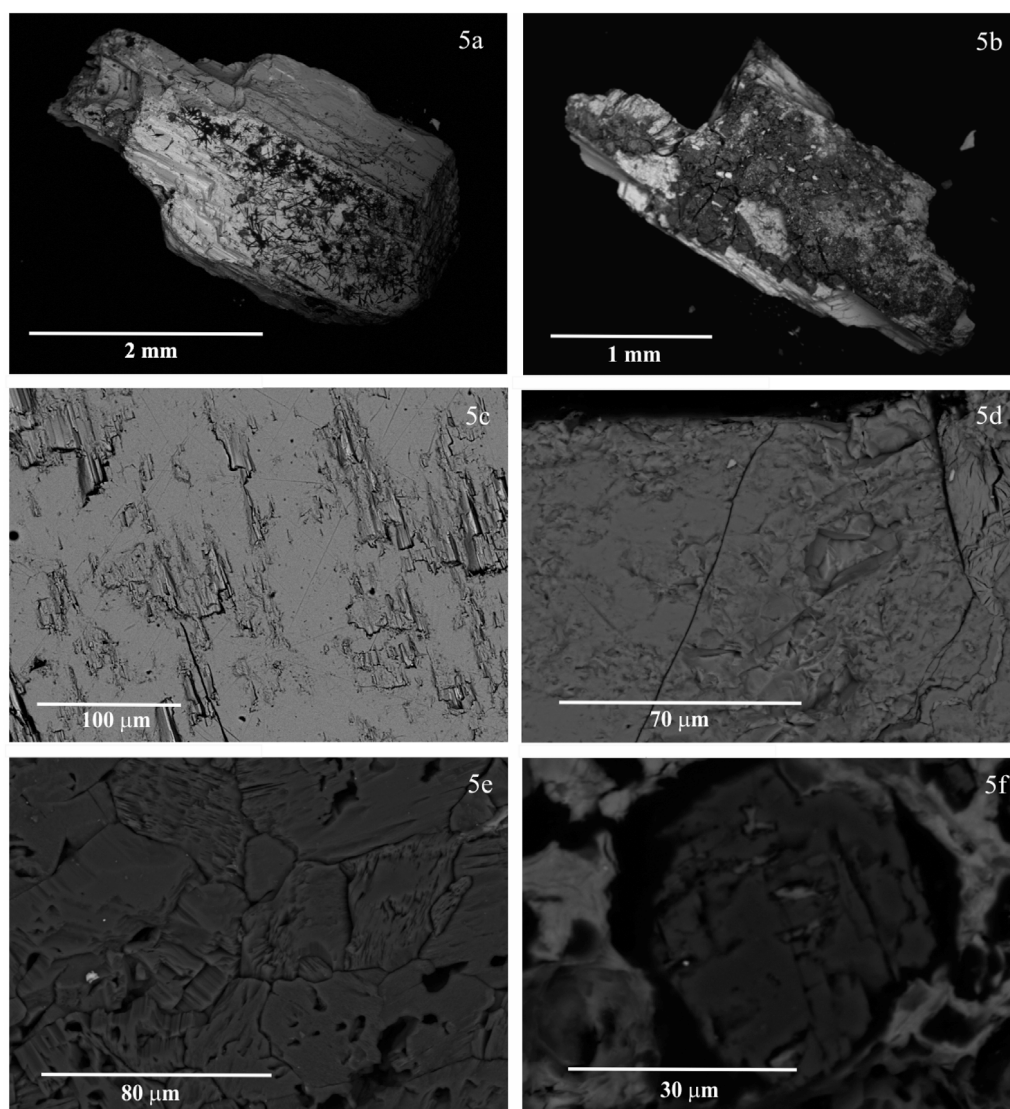
Fig. 5. a–f: BSE images of lorandite (a), realgar (b), gypsum (c), dolomite (d), unknown mineral (e), arsenates grains (f).

Table 1a
SEM-EDS analyses of pure lorandite.

Lorandite sample no.	1-1a (Lo)	1-2a (Lo)	1-3a (Lo)	1-4a (Lo)	1-5a (Lo)	1-6a (Lo)	1-7a (Lo)	2-1a (Lo)	2-2a (Lo)	2-3a (Lo)	2-4a (Lo)	2-5a (Lo)	3-1a (Lo)	3-2a (Lo)	3-3a (Lo)	3-4a (Lo)
O(%)	1.63	1.21	1.16	1.13	1.37	1.34	1.46	1.78	1.11	1.08		1.87	1.26	0.92		1.87
S	20.11	19.95	20.02	20.56	19.93	20.16	20.02	20.19	20.52	20.17	20.2	19.09	20.34	20.48	20.37	19.86
As	21.56	21.88	21.75	20.85	21.65	21.67	21.5	21.15	21.53	22.01	21.98	16.4	21.56	22.19	22.05	21.59
Tl	56.71	56.96	57.07	57.45	57.04	56.83	57.02	56.87	56.84	56.74	57.83	62.64	56.83	56.41	57.58	56.67

Lorandite sample no.	1-2a (Lo)	1-3a (Lo)	1-4a (Lo)	1-5a (Lo)	1-6a (Lo)	1-7a (Lo)	2-1a (Lo)	2-2a (Lo)	2-3a (Lo)	2-5a (Lo)	3-1a (Lo)	3-2a (Lo)	3-4a (Lo)	3-6a (Lo)	3-8a (Lo)	4-1a (Lo)
O(%)	1.21	1.16	1.13	1.37	1.34	1.46	1.78	1.11	1.08	1.87	1.26	0.92	1.87	0.91	1.22	1.15
S	19.95	20.02	20.56	19.93	20.16	20.02	20.19	20.52	20.17	19.09	20.34	20.48	19.86	21	19.89	20.32
As	21.88	21.75	20.85	21.65	21.67	21.5	21.15	21.53	22.01	16.4	21.56	22.19	21.59	22.05	21.74	21.44
Tl	56.96	57.07	57.45	57.04	56.83	57.02	56.87	56.84	56.74	62.64	56.83	56.41	56.67	56.05	57.15	57.08

Lorandite sample no.	4-4a (Lo)	4-6a (Lo)	4-7a (Lo)	5-1a (Lo)	5-2a (Lo)	5-3a (Lo)	2-4a (Lo)	3-3a (Lo)	3-5a (Lo)	3-7a (Lo)	3-9a (Lo)	4-2a (Lo)	4-3a (Lo)	4-5a (Lo)
O(%)	1.7	1.47	1.74	1.84	0.98	1.07								
S	20.62	20.9	19.83	20.22	20.12	19.83	20.2	20.37	20.59	20.41	20.66	20.69	21.43	20.06
As	21.34	21.01	21.82	21.53	21.78	21.75	21.98	22.05	22.1	22.13	22.01	21.99	22.12	22.29
Tl	56.33	56.62	56.61	56.41	57.13	57.35	57.83	57.58	57.31	57.46	57.33	57.32	56.45	57.65

Table 1b
SEM-EDS analyses of realgar and pyrite (marcasite).

Realgar sample no.	1-1b (Re)	1-4a (Re)	1-6b (Re)	1-7b (Re)	2-3c (Re)	2-4c (Re)	3-7c (Re)	4-1c (Re)	4-3c (Re)	4-5c (Re)	5-2b (Re)	Pyrite sample no.	1-3c (Py)	1-6c (Py)
O			3.3									Si		0.11
S	30.67	30.4	28.76	30.31	30.62	31.08	30.68	30.65	30.87	30.75	30.83	S	53.67	56.4
Ca	18.47											Mn		0.36
Fe			0.74	0.61								Fe	42.48	43.12
As	69.33	61.34	67.2	69.08	69.38	68.92	69.32	69.35	69.13	69.25	69.17	As	3.84	
Tl		8.26												

Table 1c
SEM-EDS analyses of gypsum and dolomite.

Gypsum sample no.	1-1c (Gi)	1-2b (Gi)	1-3b (Gi)	1-4b (Gi)	1-5b (Gi)	3-7b (Gi)	4-3b (Gi)	4-4b (Gi)	5-1c (Gi)	5-3b (Gi)	Dolomite sample no.	2-1c (D)	3-3b (D)	4-2b (D?)	4-5b (D)	4-6b (D)
O	63.27	61.27	59	60.86	60.21	59.27	59.2	59.39	59.66	60.2	O	61.3	61.78	57.82	61.51	62.15
Mg				0.3				0.87			Mg	14.35	14.67	10.69	13.5	13.99
Al			0.96			2.18	0.16				S			0.25		
Si			2.71		0.12	4.06	0.23	1.84			Ca	24.35	23.55	20.97	24.67	23.55
S	17.74	18.65	17.45	18.32	19.14	14.07	18.52	17.38	19.37	19.13	Mn			2.17		
K			0.18			0.35		0.18			Fe			5.61	0.33	0.31
Ca	18.47	19.84	18.54	20.09	20.53	15.08	20.23	18.83	20.97	20.67	As			2.5		
Mn						0.39										
Fe			0.56			1.48	0.63	0.31								
As	0.52	0.24	0.6	0.43		3.11	1.02	1.21								

Table 1d
SEM-EDS analyses of unknown phases or of phases of unknown stoichiometry.

Sample No.	1-2c	1-5c	1-7c	2-1b	2-2b	2-3b	2-4b	3-1b	3-2b	3-3c	3-4b	3-5b	3-6b	3-9b	4-1b	5-1b	5-2c
O	41.54	38.83	41.03	42.66	23.52	38.58	27.88	31.53	22.4	46.99	31.71	46.05	38.84	31.3	33.51	46.4	46.04
Na	0.58	3.13						0.58	0.47		0.9			0.51	0.63		
Mg	3.24			4.07		3.86				7.25			1.57				
Al	0.32			0.29	0.89	0.34											
Si	0.39	7.43		0.49		0.49							2.11				
P		0.5									0.68	0.78	0.43	0.65		0.6	
S	2.06	14.82	2.24	2.17	15.85	7.74	3.66	6.59	22.67			10.89	1.71	1.49	3.1	3.59	
Cl												2.85			0.37		
K		0.77															
Ca	3.2	5.81	0.29	3.82		2.38		0.31		2.06			1.31	0.31	0.69	3.41	
Ti		0.23															
Mn	1.51	0.78	5.19	5.73		0.85		0.99		3.87	0.63		6.01		0.99		
Fe	12.68	18.87	32.15	9.02	1.53	14.68	16.23	12.44	25.64	4.9	12.63	4.13	14.08	12.68	15.01	21.08	22.25
Zn		0.33		0.66		0.38				0.74							
As	34.49	8.5	19.1	31.09	17.34	30.71	18.88	26.66	19.07	34.18	26.78	13.53	33.93	24.43	29.01	24.93	31.71
Tl					40.87		31.24	20.1	9.76		26.66	21.78		28.63	16.69		

EXPLANATION:

'Unknown mineral' with the formula: $Fe_2Tl[(As_{0.85}S_{0.15})O_4]_3 \cdot 4H_2O$ (Franz et al., 1994)

Fe-Tl-arsenates (?)

Mixtures of various phases

masses of 1×10^{-6} and to high masses of $<10^{-7}$. A dual mode discrete dynode detector with 9 levels of values of linear dynamic range for the detection of the obtained ions was used. The analytical determination was performed at RF power of 1500 W, sample depth 8 mm and a carrier gas flow of 1 l min^{-1}.

The calibration was performed using a series of standard solutions prepared by the appropriate dilution of multi-element standard solutions Periodic Table mix 1 for ICP, Fluka, with a concentration of 10 mg l^{-1}, Tuning 1 Agilent with a concentration of 2.5 mg l^{-1}, and two solutions for Ti and Hg with a concentration of 1000 mg l^{-1}. The following elements were analyzed (detection limit values in ppm are given in brackets): Tl (0.05), As, Fe (10), Ca (50), Mg (50), S, Mn (0.05), Al (1), Ti (0.1), Li (0.05), Be (0.05), B (1), Na (50), P (1), K (50), V (0.05), Cr (0.05), Co (0.05), Ni (0.05), Cu (0.1), Zn (1), Ga (0.05), Ge (0.05),

Se (0.1), Rb (0.05), Sr (0.1), Mo (0.05), Pd (0.1), Ag (0.1), Cd (0.05), Sn (0.05), Sb (0.05), Cs (0.05), Ba (0.1), Hg (0.1), Pb (0.1), Bi (0.1), Th (0.1) and U (0.1).

Pure lorandite grains of the separated lorandite fraction from adit P-21 were analyzed on major and trace element contents (Table 2). In addition, seven samples of the phases that were distinguished as main impurities were also analyzed (Table 3).
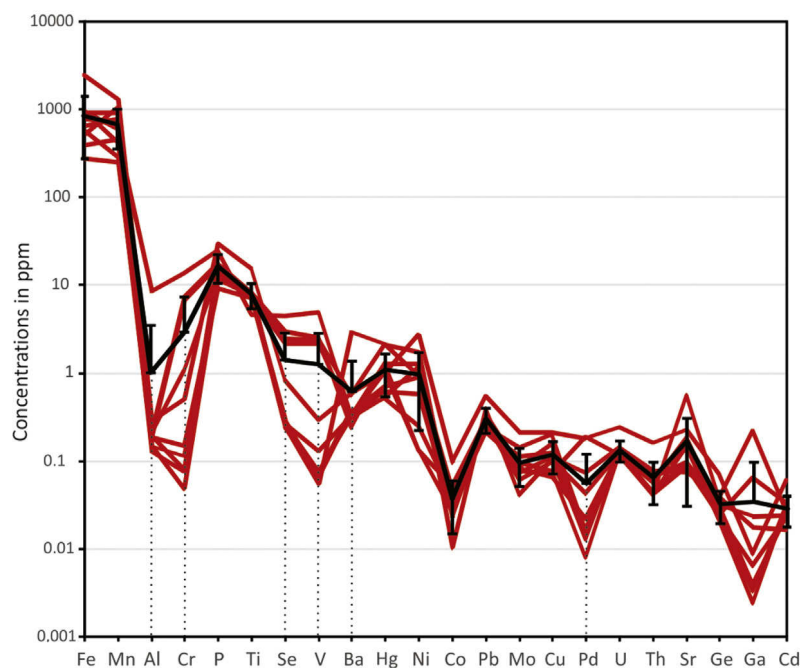
In Fig. 6, a multi-element diagram of concentrations of trace elements (above detection limit only) in lorandite separated in this study is shown. The elements are ordered in decreasing abundances in lorandite. The diagrams show average trace element concentrations for the samples separated in this study, the values for relative standard deviation (in %) as well as detection limits for each element.

Table 2

Trace elements analysis of the lorandite concentrate from adit P-21 Crven Dol; b.d.l.—below detection limit.

	Detection limit (ppm)	LV1	LV2	LV3	LV4	LV5	LV6	LV7	LV8	LV9	LV10	Aritm. mean	St.dev.	St.dev.rel
												ppm = µg/g	ppm = µg/g	%
Fe	10	793	647	944	403	923	280	2409	957	567	514	844	567	67
Mn	0.05	739	774	592	466	924	259	1304	418	282	1047	681	325	48
Al	1	b.d.l.	b.d.l.	b.d.l.	8.62	b.d.l.	b.d.l.	b.d.l.	b.d.l.	b.d.l.	b.d.l.	–	–	–
Cr	0.05	1.06	0.11	0.08	13.82	6.74	7.2	0.5	0.08	0.05	0.15	2.98	4.48	150.47
P	1	13.7	11.4	16.4	25.1	16.3	17.5	29.6	15.5	11.7	9.2	16.6	6	35.9
Ti	0.1	7.2	7.6	8.3	4.7	7.6	8.2	15.1	7.1	7.5	7.2	8	2.5	31.6
Se	0.1	2.2	0.3	0.2	4.6	2.5	3	0.8	0.3	0.3	0.2	1.4	1.5	101.4
V	0.05	2.2	0.1	0.1	5	2.4	2.6	0.3	0.1	0.1	0.1	1.3	1.6	124.5
Ba	0.1	0.3	0.3	0.4	0.3	0.6	0.2	0.6	0.3	0.4	2.9	0.6	0.8	121.2
Hg	0.1	1.3	1	0.5	0.6	2.1	1.3	1	0.5	0.7	2.1	1.1	0.6	50.7
Ni	0.05	0.1	0.1	0.2	0.6	1.8	1.3	2.7	1.2	0.9	0.9	1	0.8	77
Co	0.05	b.d.l.	0.052	b.d.l.	b.d.l.	b.d.l.	b.d.l.	b.d.l.	b.d.l.	b.d.l.	0.046	–	–	–
Pb	0.1	0.29	0.29	0.21	0.28	0.28	0.41	0.55	0.21	0.35	0.24	0.31	0.1	31.64
Mo	0.05	0.08	0.08	0.11	0.07	0.06	b.d.l.	0.21	0.1	0.09	0.14	0.1	0.05	46.06
Cu	0.1	b.d.l.	b.d.l.	0.13	0.11	0.1	0.1	0.21	0.08	b.d.l.	0.2	0.12	0.05	39.72
Pd	0.1	0.19	b.d.l.	b.d.l.	b.d.l.	b.d.l.	b.d.l.	0.18	b.d.l.	b.d.l.	b.d.l.	–	–	–
U	0.1	0.12	0.12	0.14	0.14	0.12	0.12	0.24	0.12	0.12	0.12	0.14	0.04	26.87
Th	0.1	b.d.l.	b.d.l.	b.d.l.	b.d.l.	b.d.l.	b.d.l.	0.16	b.d.l.	b.d.l.	b.d.l.	–	–	–
Sr	0.1	b.d.l.	0.15	0.1	b.d.l.	0.57	b.d.l.	0.23	0.18	b.d.l.	0.15	0.17	0.14	81.72
Ge	0.05	b.d.l.	b.d.l.	b.d.l.	b.d.l.	b.d.l.	b.d.l.	0.07	b.d.l.	b.d.l.	b.d.l.	–	–	–
Ga	0.05	b.d.l.	b.d.l.	b.d.l.	b.d.l.	0.221	b.d.l.	b.d.l.	b.d.l.	b.d.l.	0.063	–	–	–
Cd	0.05	b.d.l.	b.d.l.	b.d.l.	b.d.l.	b.d.l.	b.d.l.	0.061	b.d.l.	b.d.l.	b.d.l.	–	–	–

Fig. 6. Diagram of concentrations (ppm) of trace elements (above detection limit only) in lorandite extracted in this study. The black line shows average concentrations along with error bars showing standard deviation values.

Averaged trace element concentrations in lorandite as determined by ICP-MS in Table 2 are below 1000 ppm, *i.e.* Fe and Mn, below 100 ppm, P below 10 ppm, Al, Cr, Ti, Se, V, and Hg, below 1 ppm, *i.e.* Ba, Ni, Pb (0.31), Cu, U (0.14 ppm), and Sr, below 0.1 ppm, *i.e.* Co, Mo, Pd, Th, Ge, Ga, and Cd. The concentrations of trace elements that are significant for the feasibility of LOREX, because they can produce [205]Pb by radioactive decay, are all considerably low, *e.g.* U (~0.14 ppm), and Th (<0.1 ppm), whereas Bi concentrations are below detection limits (0.10 ppm). The samples were also analyzed by Activation Laboratories Ltd in Ancaster, Ontario, Canada. Within the experimental errors no differences to the results reported in Tables 2 and 3 could be observed.

The trace element concentrations in lorandite shown in Table 2 are lower than the concentrations in lorandite obtained by instrumental neutron activation analysis (INAA) reported by [23]. On the one hand,

the INAA analyses of lorandite revealed around ten times higher concentrations of chromium (~23 ppm), and several hundred times higher concentrations of Ni (up to 500 ppm), Cu (up to 1000 ppm) and, at smaller extent, Mo (up to 15 ppm). On the other hand, [23] reported similar concentrations of Hg but higher U and Th contents of ~1 ppm and 0.5 ppm, respectively.

In Table 3 the major and trace element contents in different most frequent impurities in lorandite as determined by ICP-MS analyses are reported and Fig. 7a–d show multi-element diagrams of trace element concentrations for seven different samples that represent most frequent impurities in the lorandite concentrate of this study. Only trace element concentrations (above detection limits) are plotted, except for coatings (type-1 and type-2), for which major element contents are also given. This was made because these samples are mixtures rather than definite mineral phases.

Table 3
ICP-MS data of major and trace element contents in different impurities in lorandite.

ppm	Gypsum	Calcite/ Dolomite	Coating type -1	Coating type -2	Unknown O-Fe-Tl-As	Realgar-1	Realgar-2
As	2300	300	15800	156100	46300	671600	616100
Tl	4100	300	26300	40700	212400	400	6200
S	150400	<1000	262200	109000	20400	29100	209300
Ca	188400	462500	10600	321900	12000	400	16200
Mg	<500	31500	<500	6100	300	<500	<500
Fe	4400	2000	260200	40200	114500	500	3700
Al	4800	14300	5100	13000	15100	<10	2300
P	1600	800	1200	2200	85200	<10	1100
Mn	400	1300	1000	4900	3500	36	500
Ti	700	1700	100	700	41	44	8
V	7.4	5.46	9.63	15.91	7.75	0.87	5.47
Cr	2.14	13.9	3.02	4.5	4.5	1.75	2.68
Zn	<10	171.29	60.51	107.63	317.87	<10	36.1
Pb	2.81	4.1	35.6	4.02	4.9	1.59	3.5
Ni	8.89	19.08	5.9	7.81	3.04	0.8	3.4
Cu	2.48	8.59	5.32	1.01	6	5.81	<1
Co	9.1	5.98	10.3	4.68	5.38	0.14	1.51
Se	1.76	2.01	2.88	1.81	1.44	2.12	2.1
Sb	0.13	0.04	7.34	1.25	7.07	30.54	7.5
Bi	<0.5	<0.5	0.37	0.05	<0.5	0.06	0.04
Th	0.63	1	6.69	2.16	<0,8	<1	<1
U	4.06	0.63	3.98	5.07	<0,9	<1	1.95
Li	0.98	5.24	1.42	2.26	<0,10	<1	1.03
Rb	2.78	0.73	2.93	4.29	<0,11	<1	1.43
Sr	23.05	256.6	1.91	29.33	<0,12	0.45	3.75
Cs	2.65	0.33	3.44	2.83	<0,13	<1	1.04
Ba	492.2	23.92	27.76	1.02	<0,14	<1	<1
Mo	1.54	<1	6.92	2.5	<0,15	<1	<1
Pd	1.99	2.17	5.27	2.43	2.21	2.07	2.16
Ag	<1	<1	48	<1	0.83	<1	<1
Cd	0.1	0.25	1.57	0.28	0.36	<1	0.16
Sn	<1	<1	<1	<1	<1	<1	<1
Be	<1	0.11	<1	0.78	1.25	<1	<1
B	<10	<10	<10	<10	<10	<10	<10
Na	<500	<500	<500	<500	<500	<500	<500
Cl	<500	<500	<500	<500	<500	<500	<500
K	<500	<500	<500	<500	<500	<500	<500
Ga	14.58	0.55	0.46	0.27	0.85	<1	<1
Ge	<1	<1	0.18	<1	<1	<1	<1
Hg	<1	<1	<1	<1	<1	<1	<1

The geochemical data show that gypsum has elevated concentrations of Tl, Al, and Fe (around 4000 ppm) and relatively high contents of P (~1600 ppm), Ti (~700 ppm), Ba (~500 ppm), and Mn (~400 ppm), whereas for all other trace elements low concentrations were obtained (Fig. 7a). For instance, the content of Th is as low as ~0.6 ppm, and the concentrations of U and Pb are ~4 ppm and ~2.8 ppm, respectively.

On the one hand, the mixture of calcite and dolomite exhibits elevated contents of Al (~1.4 wt%), as well as those of Fe, Mn, Ti, P, and S, which are the only elements with concentrations as high as, or above 1000 ppm. On the other hand, the contents of U and Th are below 1 ppm. The multi-element diagram for two types of coatings show that these two mixtures of phases are mutually compositionally similar, and that both have high concentrations of As, Tl, Al, P, Ca, Fe, and S.

Coatings type-1 display higher concentrations of Tl, P, and Ba with respect to coatings type-2, whereas the latter are more enriched in Ca, Sr and As. It is noteworthy that both types of coatings exhibit relatively uniform and slightly elevated concentrations of U (type-1: ~5 ppm,

type-2: ~4 ppm) and Th (type-1: ~2 ppm, type-2: ~7 ppm), and that is an order of magnitude higher than concentrations of these elements in lorandite (see Table 2).

The analyses of the O–Fe–Tl–As mineral display low concentrations of most trace elements and it is somewhat enriched only in Al, P, Ca, and Mn (≥1000 ppm). Frantz in [23] reported comparable (within an order of magnitude) concentrations of Sb, Mn, Co, and Mo and very similar contents of Th in, as they originally named it, the "unknown mineral" (Fig. 7). They also reported much higher concentrations of Cr (500×), Ga (four orders of magnitude), Se (300×) and U (around 10×) than in the presumably the same mineral investigated by this study.

The analyses of realgar (pure realgar: R1) and orpiment (orpiment ± realgar: R2) exhibit mutually similar trends on spider-diagram (Fig. 7d), with R2 having concentrations in excess of 1000 ppm for Tl, Al, P, Ca, and Fe. The concentrations of Th and U are very close to the detection limit. The trace element concentrations in realgar and orpiment given by [23] are generally higher than those reported in this study.
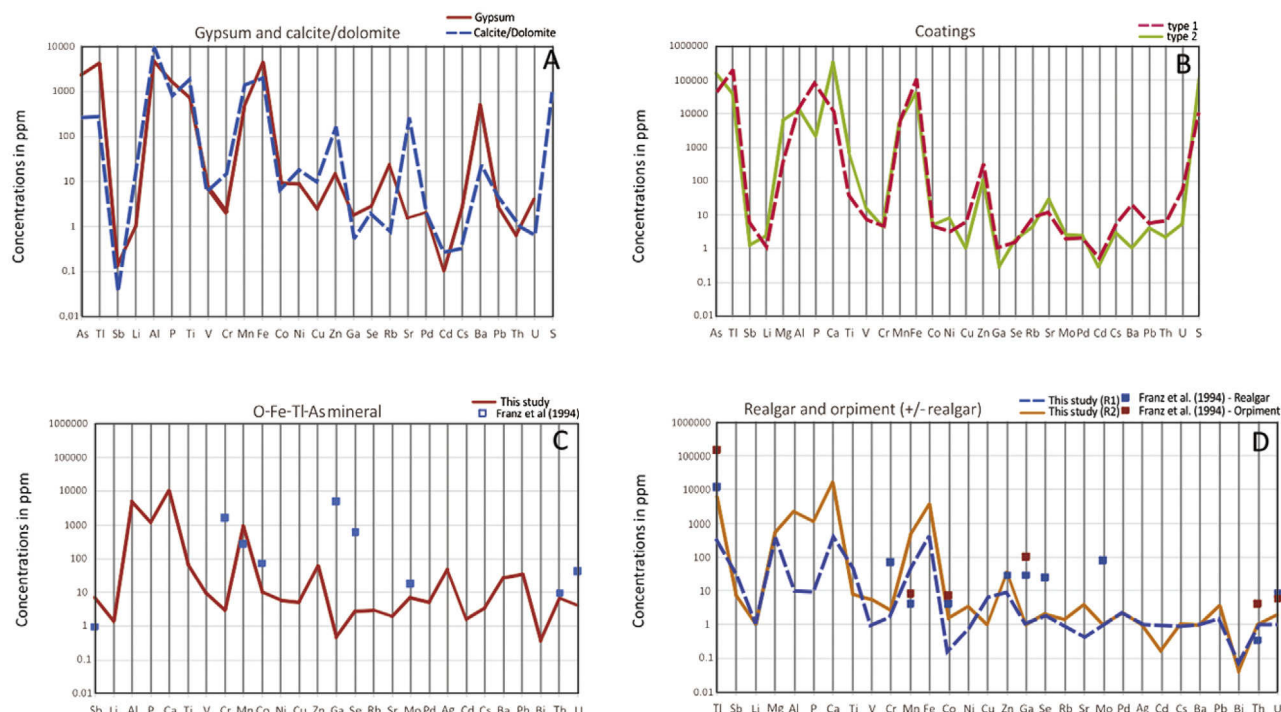
Fig. 7. A–D Diagrams of trace element concentrations for seven different samples that represent most frequent impurities in lorandite concentrate.

3.3. X-ray powder diffraction

X-ray powder diffraction patterns were recorded with a Bruker D8 Advance Da Vinci Design diffractometer (Lynx-eye solid-state detector) using Cu Kα radiation to characterize the lorandite concentrate in terms of all phases present and to determine the lattice constants. Only those lorandite crystals were used for X-ray diffraction, which had no visible coatings or inclusions of additional phases. Data were collected in the range $10° \leq 2\theta \leq 80°$. For a precise determination of the unit-cell parameter, a_0, further measurements were performed with an addition of a silicon standard with a well-known lattice constant $a_0 = 5.43088$ Å to the sample. The unit-cell parameters were determined by Rietveld refinement using the program Topas V2.1 (Bruker).

All reflections observed in the X-ray powder diffraction analysis of the lorandite concentrate could be assigned to lorandite. There is no indication of the phases observed by SEM, *i.e.* realgar, gypsum, calcite/dolomite, pyrite/marcasite or the unknown phase reported by [23] with the chemical formula $Fe_2Tl[(As_{0.85}S_{0.15})O_4] \times 4H_2O$ or any other mineral. Therefore, the lorandite concentrate is considered as pure-phase, according to the results of X-ray powder diffraction, *i.e.* the content of impurity phases should be below 1%.

The lattice constants were determined to be $a = 12.29602(60)$ Å, $b = 11.31497(62)$ Å, $c = 6.11073(44)$ Å, and $\beta = 104.2527(60)°$. These parameters compare quite well with those reported by [24], *i.e.* $a = 12.293$ Å, $b = 11.306$ Å, $c = 6.111$ Å and $\beta = 104.26°$, also determined from a lorandite sample from Allchar.

4. Discussion

The above presented results of SEM-EDS and ICP-MS characterization of individual grains and various fractions of pure lorandite and minerals that occur as impurities in lorandite have significant implications on the future activities of LOREX. In the following text we briefly discuss the quality of the separated lorandite concentrate and, in the same context, the overall efficiency of the so far applied (and still ongoing) method of lorandite extraction.

4.1. The efficiency of the method of lorandite separation

The above discussion provides conditions to assess the suitability of the ongoing method of lorandite extraction from the raw ore from adit P-21 Crven Dol. The main question that needs to be answered is whether the ongoing method is appropriate for producing enough quantities of sufficiently clean and pure lorandite concentrate? The answer on this question is essential for the future of the LOREX project.

It is inevitably clear that both pilot experiments according to the methods of [22] were not successful in producing satisfactory results (see 2.1.2). They involved almost complete mechanical processing of ore, which caused the loss of most coarse-grained crystals of lorandite. These very soft crystals were removed as mud fraction during processing and any subsequent gravitational separation was not able to counterbalance this loss. According to rough calculations, the pilot experiment 1 produced only 20 g of lorandite concentrate (around 60% of purity) out of almost more than 500 g of available lorandite.

The problem of unwanted loss of coarse and soft lorandite crystals has been fully addressed by the method of separation applied in this study. It involved an entirely manual crushing and grinding and, therefore, increased the quantity of produced concentrate.

4.2. The purity of the separated lorandite concentrate

The method applied in this study, however, produces lorandite crystals that are not entirely free of impurities but may contain coatings and very tiny intergrowths and inclusions, among which predominate realgar, orpiment, gypsum, calcite/dolomite, an O–Fe–Tl–As mineral as well as various sulfates and arsenates. Petrographical observations under binocular lens suggested that the amount of impurities are below 1% or even lower. This is confirmed by the results of X-ray powder diffraction, which exhibit no indications of extra or impurity phases and therefore their amount is considered to be below 1%.

The qualitative SEM-EDS characterization and the subsequent quantitative analyses indicate that the lorandite concentrate produced in this study consists of pure crystals of lorandite that contain minor amounts of impurities below 1%. The results show that the inclusion-

and coatings-free crystals of lorandite display homogeneous BSE images and exhibit relatively uniform major element compositions. There are only minimal deviations from the ideal stoichiometric composition of lorandite, although most grains contain some oxygen in the range of 1–2 wt%. The analyses showing oxygen have also nearly stoichiometric Tl/As and Tl/S ratios. The latter indicates that the presence of oxygen is not an analytical problem, but most likely the consequence of incipient oxidation of lorandite. It is in accordance with petrographical observations, that in some ores lorandite is partly to totally altered into yellow dust-like aggregates.

A larger variability of trace element data for lorandite is present only for elements that are very close to detection limits, and this can be regarded as geochemically insignificant. The most significant information from these data is that the studied lorandite exhibits only higher average concentrations of Fe, Mn, P, Ti, and Cr. The higher concentrations of these elements can be related to the presence of submicroscopic impurities and the most suitable candidates are both types of coatings (type-1 and type-2) and the O–Fe–Tl–As mineral. The contribution of all other impurities was most likely extremely small, in any case insufficient to produce measurable geochemical effects. For instance, even very small quantities of gypsum (<0.1%) would increase calcium contents in lorandite above the detection limit, and this was not revealed by the ICP-MS analyses.

However, despite of all these considerations it should be emphasized that the contents of the critical elements U (0.14 ppm), and Th (0.1 ppm), which can also produce ^{205}Pb by radioactive decay, and thereby contribute to the background events, are below 0.25 ppm in lorandite. The other element producing ^{205}Pb by radioactive decay, *i.e.* Bi, is even below the detection limit of ICP-MS analysis (<0.1 ppm). Therefore, the contribution of these elements to the background in lorandite can be regarded as negligible. The amount of the critical elements in the impurities in lorandite is very low, *i.e.* U below 6 ppm, Th below 7 ppm, Bi below 1 ppm (cf. Table 3). If the very low amount of impurities in the lorandite concentrate, *i.e.* below 1%, and in addition the very low amount of critical elements in these impurities are considered, it can be concluded that their contribution to the background events can be neglected.

5. Conclusions

The complex procedure of ore extraction and lorandite separation, which is described in this study, was successful in obtaining a concentrate of 400 g pure lorandite out of an amount of 10.5 tons of raw ore. The applied process of lorandite separation was carried out without chemical treatment, i.e. under contamination-free conditions, and produced a concentrate of very high-purity lorandite in which the presence of impurities is estimated as <1%. Given that the increase in quantity of pure lorandite proportionally decreases the error in the estimate of ^{205}Pb as the main signal of pp-neutrino detector, this represents a significant contribution to the successful realization of the LOREX Project.

The lorandite crystals themselves are very homogeneous and pure with almost stoichiometric composition. For the total lead concentration in lorandite a value of 0.31 ppm has been found. Such low Pb concentrations are also favorable for the LOREX feasibility. Taking into account the present day absolute detection limit of ^{205}Pb of $\delta_a \leq 1 \times 10^{-3}$, these low Pb concentrations in lorandite allow for obtaining reliable measurements with ca. 1 kg of such a lorandite concentrate.

The contents of the critical elements in lorandite, which can produce ^{205}Pb by radioactive decays, *i.e.* U, Th, and Bi, and thereby contribute to the background events, are very low, *i.e.* <0.25 ppm and therefore their influence can be neglected.

Therefore, from the viewpoint of mineralogy, geochemistry, and ore processing, it can be concluded that the lorandite concentrate is well suited for the exact determination of the ^{205}Pb concentration in lorandite.

Thus from the geochemical point of view, the whole LOREX experiment has a good chance to be successful.

References

[1] J.A. Krenner, Lorandite, ein neues Thallium Mineral von Allchar in Mazedonien, Math. és term. tud. Értesitö 12 (1894) (1897) 473–479; 13 (1895) 258–263 (Hungarian); Z. Kryst. 27 98–99.

[2] J.W. Anthony, R.A. Bideaux, K.W. Bladh, M.C. Nichols (Eds.), Handbook of Mineralogy, Mineralogical Society of America, Chantilly, VA, USA, 2003, pp. 20151–21110.

[3] M.S. Freedman, C.J. Stevens, E.P. Horwitz, L.H. Fuchs, J.L. Lerner, L.S. Goodman, D.J. Childs, J. Hessler, Solar neutrinos: Proposal for a new test, Science 193 (1976) 1117–1118.

[4] M.K. Pavićević, Lorandite from Allchar –a low solar neutrino dosimeter, Nucl. Instrum. Methods Phys. Res. A 271 (1988) 287–296.

[5] M.K. Pavićević, The "LOREX" –project, solar neutrino detection with the mineral lorandite (progress report), Neues Jahrb. Mineral. Abh 167 (1994) 205–245.

[6] M.S. Freedman, ^{205}Tl as a low energy neutrino detector, in: G. Friendlander (ed.), Proceedings of the Informal Conference on Status and Future of Solar Neutrino Research, Vol. 1, BNL Report 50879, 1979, pp. 313–360.

[7] G. Audi, F.G. Kondev, M. Wang, W.J. Huang, S. Naimi, The NUBASE2016 evaluation of nuclear properties, Chin. Phys. C 41 (2017) 030001.

[8] F. Neubauer, M.K. Pavićević, J. Genser, R. Jelenković, B. Boev, G. Amthauer, ^{40}Ar/^{39}Ar dating of geological events of the Allchar deposit and its host rock, Geochim. Cosmochim. Acta 73 (Suppl. 1 A) (2009) 938.

[9] M.K. Pavićević, F. Bosch, G. Amthauer, I. Aničin, B. Boev, W. Brüchle, Z. Djurčić, T. Faestermann, W.F. Henning, R. Jelenković, V. Pejović, New data for the geochemical determination of the solar pp-neutrino flux by means of lorandite mineral, Nucl. Instrum. Methods Phys. Res. A 621 (2010) 278–285.

[10] P. Kienle, Studies of radioactive decays of completely ionized nuclei in a heavy ion storage ring, Nucl. Instrum. Methods Phys. Res. A 271 (1988) 277–279.

[11] F. Bosch, Yu.A. Litvinov, T. Stöhlker, Nuclear physics with unstable ions at storage rings, Prog. Part. Nucl. Phys. 73 (2013) 84–140.

[12] B. Boev, Petrological, Geochemical and Volcanic Features of Volcanic Rocks of the Kožuf Mountains (Ph.D. thesis), Faculty of Mining and Geology, Štip, 195 p., 1988 (in Macedonian).

[13] S. Jankovic, The Allchar Tl-As-Sb deposit, Yugoslavia and its specific metallogenic features, in: E. Nolte, M.K. Pavićević (Eds.), Solar Neutrino Detection. Proceed. Int. Conf. on Solar Neutrino Detection with ^{205}Tl and Related Topics, North-Holland, Amsterdam, 1988, p. 286.

[14] S. Janković, R. Jelenković, Thallium mineralization in the Allchar Sb–As–Tl–Au deposit, Neues Jahrb. Miner. Abh. 167 (1994) 283–297.

[15] G. Amthauer, M.K. Pavićević, R. Jelenkovic, A. El Goresy, B. Boev, P. Lazic, State of geoscientific research within the lorandite experiment (LOREX), Mineral. Petrol. 105 (2012) 157–169.

[16] S.M. Schmidt, D. Bernoulli, B. Fügenschuh, L. Matenco, S. Schefer, R. Schuster, M. Tischler, K. Ustaszewski, The Alps–Carpathians–Dinarides-connection: a correlation of tectonic unit, Swiss J. Geosci. 101 (2008) 139–183.

[17] S. Janković, B. Boev, T. Serafimovski, Magmatism and tertiary mineralization of the Kozuf metallogenic district, the Republic of Macedonia with particular reference to the Alsar deposit. Univ. "St. Kiril and Metodij" - Skopje, Faculty of Mining and Geology, Geological Department, Special Issue No. 5, 1997, p. 262.

[18] M. Troesch, E. Frantz, ^{40}Ar/^{39}Ar Alter der Tl-As Mine von Crven Dol, Allchar (Macedonien), Beihefte Eur. J. Miner. 41 (1992) 276.

[19] M.K. Pavićević, V. Cvetkovic, S. Niedermann, V. Pejovic, G. Amthauer, B. Boev, F. Bosch, I. Anicin, W.F. Henning, Erosion rate study at the Allchar deposit (Macedonia) based on radioactive and stable cosmogenic nuclides (^{26}Al,^{36}Cl,^{3}He, and ^{21}Ne), Geochem. Geophys. Geosyst. 17 (2016) 410–424.

[20] M.K. Pavićević, F. Bosch, G. Amthauer, I. Aničin, B. Boev, W. Brüchle, V. Cvetković, Z.Đ. určić, W.F. Henning, R. Jelenković, V. Pejović, A. Weiss, Status and new data of the geochemical determination of the pp-neutrino flux by LOREX, Adv. High Energy Phys. (2012) Art. ID 274614, 15 p.

[21] H. Wagner, The new Austrian tunneling method, Technol. Potential Tunnel. 6 (1970) 81–84.

[22] B. Petrov, D. Andonova, T. Stafilov, T. Novakovski, Possibilities of concentration thallium mineral lorandite from the Allchar deposit, Crven Dol Region, Neues Jahrb. Mineral. Abh. 167 (1994) 413–420.

[23] E. Frantz, H. Palme, W. Todt, A. El Goresy, M.K. Pavićević, Geochemistry of Tl-As minerals and host rocks at Allchar (FYR Macedonia), Neues Jahrb. Mineral. 167 (1994) 359–399.

[24] A. Zemann, J. Zemann, Zur kenntnis der kristallstruktur von lorandit TlAsS2, Acta Crystallogr. 12 (1959) 1002–1006.